# Phase separation dynamics in wetting ridges of polymer surfaces swollen with oils of different viscosities

Zhuoyun Cai<sup>1,†</sup>, Rodrique G. M. Badr<sup>2,†</sup>, Lukas Hauer<sup>3</sup>, Krishnaroop Chaudhuri<sup>4</sup>, Artem Skabeev<sup>5</sup>, Friederike Schmid\*<sup>2,2</sup>, and Jonathan T. Pham\*<sup>4</sup>

<sup>1</sup>Chemical and Materials Engineering, University of Kentucky, Lexington, KY 40506, USA <sup>2</sup>Institut für Physik, Johannes Gutenberg Universität Mainz, Staudingerweg 7, 55099, Germany <sup>3</sup>Institute for Biology, Humboldt-Universität zu Berlin, 10115, Berlin, Germany <sup>4</sup>Chemical and Environmental Engineering, University of Cincinnati, Cincinnati, OH 45221, USA <sup>5</sup>Institute of Organic Chemistry and Macromolecular Chemistry, Friedrich Schiller University Jena, Lessingstrasse 8, 07743 Jena, Germany

#### **Abstract:**

When drops are placed on a sufficiently soft surface, the drop surface tension drives an out of plane deformation around the contact line (i.e., a wetting ridge). For soft elastomeric surfaces that are swollen with a liquid, capillarity from a drop can induce a phase separation in the wetting ridge. Using confocal microscopy, we study the dynamics of phase separation at the wetting ridge of glycerol drops on silicone elastomers, which are swollen with silicone oils of varying viscosity (i.e., molecular weight). We show that the viscosity of the swelling oil plays a large role in the oil separation size and separation rate. For networks swollen to near their maximum swelling (i.e., saturated), lower viscosity oil separates more and separates faster at early times compared to larger viscosity oil. During late-stage wetting, the growth rate of the separation is a function of viscosity and swelling ratio, which can be described by a simple diffusive model and a defined wetting ridge geometry. In this late-stage wetting, the higher viscosity oil evidently grows faster, likely because it is further from reaching equilibrium. Interestingly, the separated oil phase region grows with a nearly constant, geometrically similar shape. Understanding how phase separation occurs on swollen substrates should provide information on how to control drop spreading, sliding, adhesion, or friction on such surfaces.

<sup>&</sup>lt;sup>†</sup> Equal contribution

<sup>\*</sup>E-mail: Jonathan.Pham@uc.edu, friederike.schmid@uni-mainz.de

#### Introduction

Wetting on soft surfaces has gain significant attention for the wide range of potential applications, from soft robots<sup>1</sup> and biological processes<sup>2</sup> to adhesives and self-cleaning coatings.<sup>3,4</sup> Drops on soft elastomers generate an out-of-plane deformation around the three-phase contact line, known as a wetting ridge, due to the drop surface tension pulling vertically on the surface<sup>5-9</sup>. Such behavior is more easily observed when the modulus of the polymer network is soft enough for surface tension to cause visible deformations. This ridge can play a role in drop spreading, drying, and sliding<sup>10–18</sup>. Similarly, wetting ridges can also be found on slippery, lubricant-infused surfaces, although these ridges are comprised purely of liquid lubricant<sup>19–23</sup>. Swollen elastomers, which are polymer networks infused with a liquid, can behave as an intermediate between these two cases; the swelling liquid can separate from the polymer network, making the wetting behavior even more complex<sup>24–39</sup>. Specifically, when a drop is placed on a swollen elastomer, the imbibed liquid may phase separate at the contact line, affording a pure liquid phase at the wetting ridge tip<sup>15,35,40,41</sup>. While wetting-induced phase separation on swollen elastomers has been investigated, the shape and growth dynamics of the phase separated region is not well understood, especially as a function of the swelling liquid viscosity. Such information is critical for designing timedependent processes for soft polymer coatings.

To study soft wetting, silicone elastomers (e.g., crosslinked polydimethylsiloxane, PDMS) are one of the most widely used substrates,<sup>31</sup> due to their commercial availability, easily tuned modulus, and simple preparation methods.<sup>11,25,40,42-47</sup> However, many elastomers contain uncrosslinked molecules (i.e. extractable oils) that are left over after curing, which serve as a liquid swelling agent in the network<sup>48–50</sup>. Hence, these materials are two-component systems that include a crosslinked network and an uncrosslinked liquid; the liquid phase is effectively a high viscosity silicone oil. For example, the Sylgard 184 elastomer kit has a base liquid polymer with a viscosity of ~5000 cSt, which likely makes up most of the remaining extractable oil in the elastomer after curing<sup>48,51,52</sup>. This high viscosity oil can play an important role in dynamic surface properties, like drop sliding dynamics<sup>53</sup> and adhesive detachment dynamics<sup>54</sup>. However, prior studies have not investigated the phase separation shape and dynamics with varying oil viscosities.

In this work, we study the dynamics of wetting-induced oil phase separation of on lightly crosslinked elastomers near the contact line of a liquid drop (Figure 1a). We focus on how the oil viscosity (i.e., molecular weight) and the degree of swelling (i.e., amount of infused oil) affects the size and growth rate of the separated oil region (Figure 1b-1c). For highly swollen networks, the oil separation size increases with time after a drop is placed on the surface. The separation occurs faster at early times and then slows at longer times. For intermediately swollen elastomers, the oil separation size reaches a maximum and remains constant with time. The separation rate is a function of the oil viscosity; lower viscosities separate more and faster at early stages, while the ridge growth is faster for higher viscosity during later stages. Interestingly, we observe that the growth of the oil region grows with a consistent geometry that scales up during growth. Our result suggests that phase separation size and rate are strongly affected by the viscosity and

amount of oil in soft elastomers, which may provide insight into the design of soft polymer coatings.

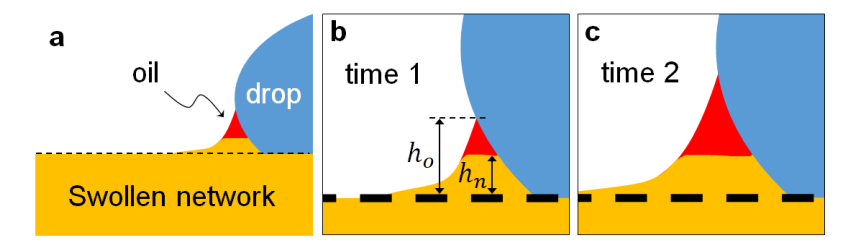


Figure 1: Schematic diagram illustrating the experiment. (a) A drop is placed on swollen elastomer, creating a zone of oil separation near the contact line. (b-c) Zoomed-in regions of the contact line at two different time points. The oil  $(h_o)$  and network heights  $(h_n)$  are measured over time, with the separation height given by  $\Delta h = h_o - h_n$ . At an early time point (e.g. time 1), there is a small amount of oil separation. At a later time point (e.g. time 2), the  $h_n$  remains constant and  $h_0$  increases. Note that the wetting ridge zone is not to scale and serves only to describe the process.

#### Results and discussion

Surfaces with different viscosity oils. To prepare our surfaces, we use a commercially available polydimethylsiloxane (PDMS) elastomer kit (Sylgard 184, Dow) with a base to crosslinker ratio of 60:1 by weight; this leads to an as-prepared Young's modulus of the order ~5 kPa<sup>32,46,55</sup>. At this high base/crosslinker ratio (noting that the manufacturer recommended ratio is 10:1, modulus ~1 MPa), the base is in excess relative to the crosslinker, resulting in uncrosslinked chains that remain in the as-prepared samples after curing. The properties of the uncrosslinked chains are generally unknown because they come from a commercial product and because there is limited control over the molecular weight distribution and architecture after curing. To control the number and molecular weight of free chains, we first remove these uncrosslinked chains by washing samples in hexane. In this procedure, the as-prepared samples are immersed in hexane for several days to allow the uncrosslinked chains to migrate from the elastomer into the surrounding solvent. The process is repeated three times. The washed elastomers are then dried to remove residual hexane; we consider these washed samples as dry polymer networks. Details of this washing process are described elsewhere. 40,48

To study the effect of oil viscosity, the dry samples are swollen with different silicone oils. We use unreactive, trimethylsiloxy-terminated silicone oils with molecular weights of 14 kg/mol, 28 kg/mol, and 49 kg/mol, which have viscosities of 350, 1000, and 5000 cSt, respectively. To measure the maximum degree of swelling for the different molecular weights, we prepare dry blocks of 60:1 PDMS (1.5 x 1 cm x 1 mm) and subsequently immerse them in oil. Upon immersion, the oil penetrates the network until it reaches a maximum degree of swelling (i.e., saturated). The degree of swelling is defined as  $Q = V_d/V_s$ , where  $V_d$  is the volume of the dry sample and  $V_s$  is the volume of the swollen elastomer. For all molecular weights, Q increases with immersion time, indicating

that silicone oil expands the PDMS elastomer (Figure 2). The rate of increase in Q is fast initially and slows down in the range of 25-50 days, although Q continues to increase after 135 days (~4.5 months). As anticipated, the maximum degree of swelling and the rate of swelling decrease with increasing molecular weight. At 135 days, Q~4.0 for 14 kg/mol oil, ~2.9 for 28 kg/mol oil, and ~2.0 for 49 kg/mol oil. Q appears to be approaching a maximum at 135 days. The increase in swelling over these long times may be due to the slow reaching of equilibrium by swelling thick samples with high viscosity oil or possibly due to chains breaking (e.g. hydrolysis) and altering the equilibrium swelling ratio. Nevertheless, since these values are approaching a plateau, we assume these are around their saturated swelling states, and will be used as a baseline comparison for preparing swollen, micron-scale thick films for the following wetting experiments. It should be noted that due to challenges in high viscosity swelling (i.e., long saturation times) and sample preparation of thin films of micron-scale thickness, some variations exist in the maximum measured Q in the following samples for wetting experiments.

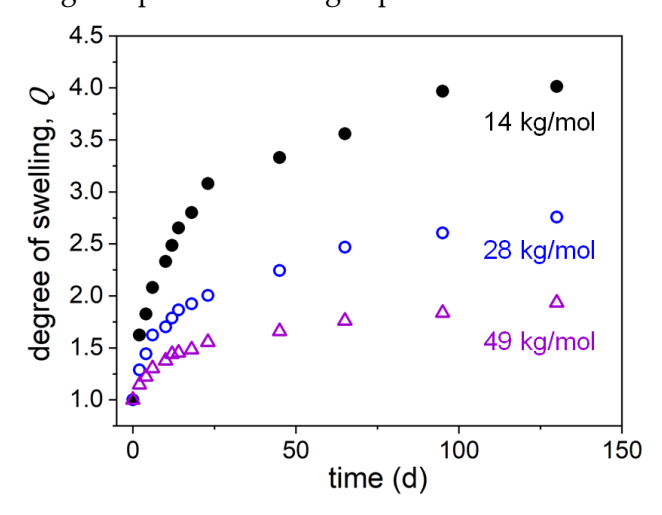


Figure 2. The degree of swelling Q as a function of immersion time in days for macroscopic, bulk PDMS elastomers being swollen with silicone oil having molecular weights of 14 kg/mol, 28 kg/mol, and 49k g/mol.

Observing time-dependent phase separation. To investigate the wetting ridge at the periphery of a drop, a glycerol drop is placed onto the surface while imaging its contact line. Glycerol is used because it has a similar surface tension to water, low volatility, and does not swell or mix well with PDMS<sup>51</sup> or silicone oil<sup>56</sup>, which are important for long wetting experiments. Moreover, we previously found that the spreading parameter S should be positive for oil separation to occur spontaneously<sup>31,40</sup>; S > 0 for a glycerol and silicone oil system. In Fig. 3a, confocal images are presented for a drop on a surface with 14 kg/mol oil and a measured swelling of Q = 4.1 (~maximum swelling). At early stages (30 s), the swollen polymer network is pulled up and a small amount of oil separation is visible. This suggests that the emergence of the phase separated region is a fast process. One can hypothesize that at initial contact (t=0), the drop interfaces with both polymer network chains and oil molecules. Shortly after, the oil separates and the vertical interfacial stresses at the tip of the ridge are mostly felt by the phase separated oil region. After

50 minutes (3000 s), more oil separates, while it appears that the polymer network relaxes in the vertical direction. After an even longer time of 5 hours (18000 s), the oil separation becomes more apparent. Additionally, it is observed that not only does the height of the distinct oil wetting ridge grow over time, but so does the width to the same extent; that is, the shape remains geometrically similar.

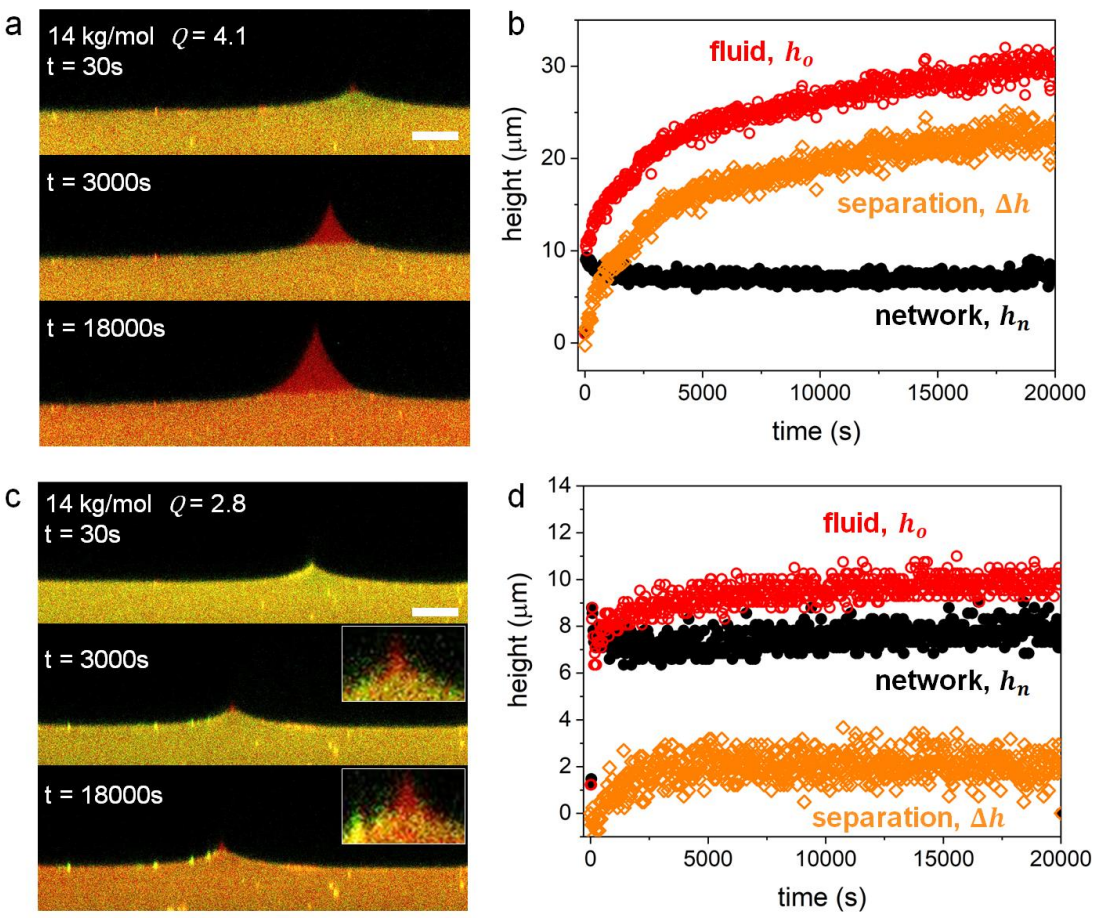


Figure 3. (a,c) Confocal imaging of oil separation during wetting of a glycerol drop on PDMS elastomers swollen with 14 kg/mol silicone oil. The insets in (c) are to illustrate oil separation more clearly at these low separations. (b,d) The corresponding measured heights are plotted. The degrees of swelling Q are (a-b) 4.1 and (c-d) 2.8. Scale bar: 20  $\mu$ m.

To gain more insight into this time-dependent process, we measured the maximum network height  $h_n$  and the oil tip height  $h_o$  relative to the original, unperturbed surface. The separation size is calculated from these values, defined as  $\Delta h = h_o - h_n$ . These heights are presented in Fig. 3b for the corresponding images in Fig. 3a. Consistent with our confocal images, the oil separation size increases as a function of time. In the short time regime (e.g. 30 s), a quick formation of the network wetting ridge is observed when the drop is placed, while a very small  $\Delta h$  is observed. However,  $h_o$  increases with increasing time. After 3000 s,  $\Delta h \approx 16 \,\mu\text{m}$ , and reaches  $\approx 30 \,\mu\text{m}$  at 18000 s. This qualitative trend also holds for a polymer network swollen to a lower swelling of Q = 2.8 (Fig. 3c), but with smaller $\Delta h$ . In this case, we find again that the network wetting ridge

forms quickly, but without clear oil separation at t=30 s. After 3000 s, a small amount of oil separation can be visualized, which appears to be maintained after 18000 s. This is evident in Fig. 3d, which shows that the separation size  $\Delta h$  reaches ~2  $\mu$ m after about ~2500 s; thereafter it does not increase significantly with time (Figure 3c-d). This concept of a stable  $\Delta h$  is consistent with our prior work on low molecular weight oils (770 g\mol), which showed an apparently stable oil separation after a few minutes<sup>40</sup>. When the degree of swelling is decreased even more to Q=2.1, effectively no oil separation is visible in our confocal images. The data becomes rather noisy, and the oil and network heights are difficult to discern. It is likely that a small amount of oil does separate, which is outside the resolution limit of our confocal microscope.

To investigate the idea of geometric similarity in the ridge, we trace the ridge shapes at different times and overlay them. Fig. 4a shows the shapes of the ridge for 14 kg/mol oil at the highest swelling for all times. The lines are colored according to the measurement time, gradually changing from dark purple at early times to light yellow at the latest time. To show the similarity in the shape, we rescale the ridges at different times to have the same ridge height, as measured from the unperturbed surface of the network. Fig. 4b shows the ridge at different times after rescaling. As it turns out, the ridge initially steepens with time (illustrated by the outlying purple lines), but soon assumes an invariant shape. Except for the outlying early times, we see a collapse of the shapes after rescaling. At equilibrium, a self-similar shape is expected to appear as the result of a point load on a viscoelastic medium<sup>57</sup>, and we believe this manifests itself in the geometrically similar growth of the liquid ridge at steady state. To further characterize the shape during growth, we measure the opening angle at the tip of the separated ridge (i.e., the tip of the oil-water-air contact line). We take the 30 points closest to the tip of the ridge from either side and fit each to a line, giving an approximation for the left and right tangents. The opening angle is then calculated as the angle between those lines. The results for 14 kg/mol are shown in Figs. 4c and 4d at Q=2.8and Q = 4.1, respectively; the angles relax and take constant values after about 500 s and 1000 s, respectively. Both durations are shorter than the time needed to reach equilibrium, which is about 2500 s for Q = 2.8, and longer than 20000 s for Q = 4.1. The steady value for the measured angle further supports the similarity in the ridge shape during growth.

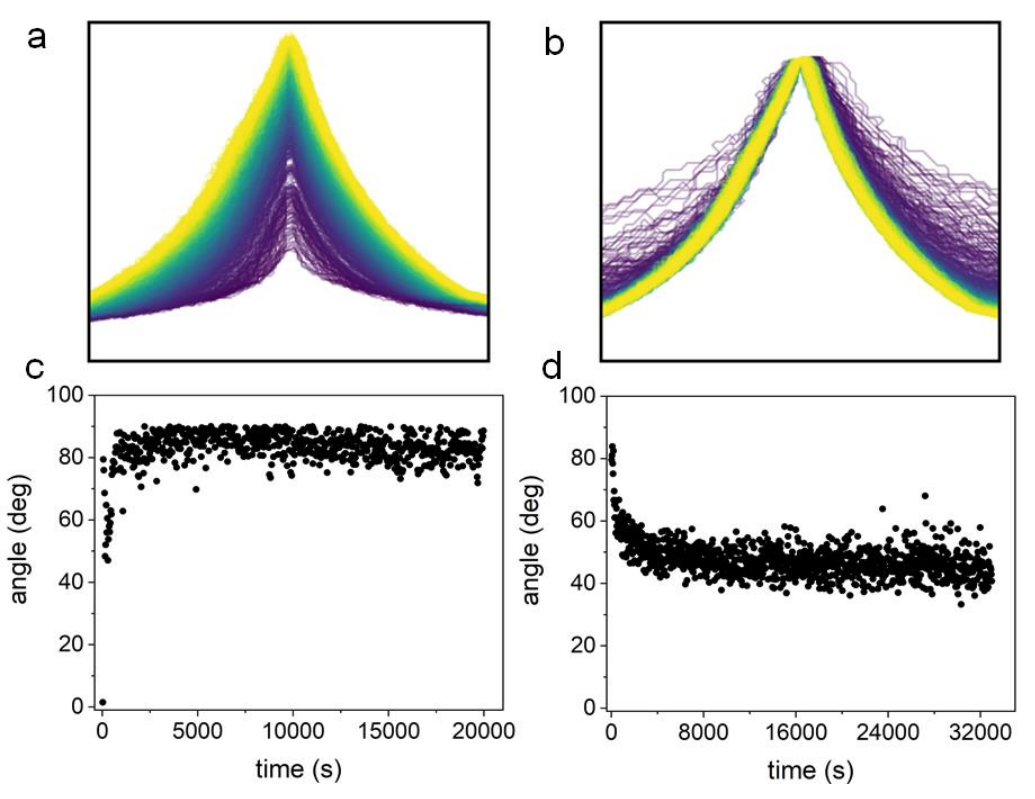


Figure 4. Geometry of the wetting ridge for 14k and Q = 4.1. (a) Original ridge and (b) rescaled ridge at all times. The time span between two lines is about 30 s, and the lines are colored according to the measurement time, gradually from dark purple at early times to light yellow at the latest time. Except for ridges at early times, the ridge shapes collapse to a common one after rescaling. (c-d) Opening angles of the oil ridge tip for 14k oil swollen surfaces for (c) Q = 2.8 and (d) Q = 4.1. The opening angle is measured using estimates of the tangents from both sides of the tip of the ridge.

An interesting point is that the tip angle is relatively large (>40°). Due to the interfacial tensions at play in our system, vanishingly small angles are expected. The reason is because the spreading parameter of the oil on the glycerol is positive, meaning that at equilibrium, a Neumann configuration is not possible.<sup>31</sup> In addition, if the network is highly swollen, the oil likely cloaks the drop, leading to a vanishing angle at the tip of the ridge. Measuring angles from microscopy images suffers from inherent limitations, namely the imaging resolution and the inability of image analysis tools to find infinitely sharp corners in noisy images. This may lead to measured angles being larger than they are in reality. The reported angles should, therefore, not be taken as a sign of the existence of a stable Neumann state at equilibrium, but simply as an indication of the similarity of the shape of the ridge during growth.

To compare the oil separation for the different molecular weights,  $\Delta h$  for different Q are plotted for the 14, 28, and 49 kg/mol surfaces as a function of time (Figs. 5a-c). In the 14 kg/mol case, the sample with high swelling (Q = 4.1) displays a large separation size, which decreases with

decreased swelling. Hence, the maximum separation size is a function of the degree of swelling. The same general trend is observed for the 28 kg/mol and 49 kg/mol oils (Fig. 5b-c); when the networks are swollen to their maximum values, a large oil separation is observed ( $Q_{max} = 3.5$  for 28 kg/mol and  $Q_{max} = 2.3$  for the 49 kg/mol), which decreases with decreased swelling. This can be conveniently observed in Fig. 5b for the 28 kg/mol samples, where the long time  $\Delta h$  decreases with decreasing Q. At a sufficiently low Q, the separation size  $\Delta h$  becomes too small to clearly image. For example, samples with Q = 1.9 for the 28 kg/mol and Q = 1.4 for the 49 kg/mol do not display clear separation, even after a long wetting time of ~5 hours; the values remain around ~1  $\mu$ m with noisy data, close to our resolution limit. This little to no oil separation is consistent with our previous study suggesting that the fluid is held inside the polymer network for elastomers with a low Q, possibly due to osmotic pressure.  $^{16,24,39,40}$ 

To make a direct comparison between the different viscosity oils, we replot the highest swelling data from Figs. 5a-c in Fig. 5d; during the duration of our experiments, the separation size clearly increases with decreasing oil molecular weight. However, we note that the lower molecular weight system has a larger absolute amount of oil within the network, since it has a higher maximum Q (Fig. 2). Hence, it is not immediately obvious whether the molecular weight or the amount of oil in the network governs the oil separation size. One could also compare samples with similar degrees of swelling but different molecular weights (e.g. Q = 2.3 for 49 kg/mol, Q = 2.5 for 28 kg/mol, and Q = 2.8 for 14 kg/mol, Fig. 5a-c); however,  $\Delta h_{max}$  for these are not similar. For example, although the swelling ratio for 49 kg/mol is the lowest (Q = 2.3), the ridge height reaches higher values than for 28 kg/mol (Q = 2.5), followed by 14 kg/mol, which has the highest swelling ratio of the three (Q = 2.8). These overall results indicate that even though the swelling ratio plays a role in  $\Delta h_{max}$ , it is also strongly governed by the viscosity.

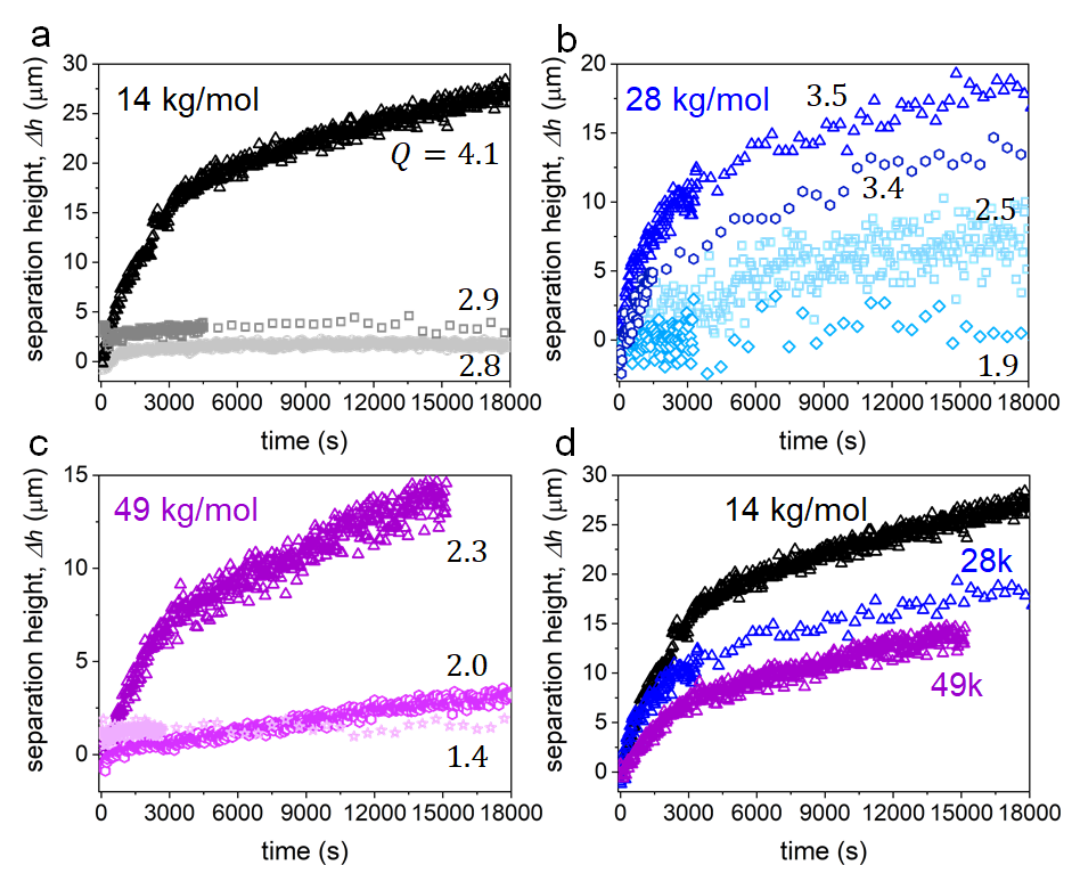


Figure 5. Separation height  $\Delta h$  as the function of wetting time with different degrees of swelling Q for PDMS elastomers swollen with silicone oil having molecular weights of (a) 14, (b) 28, and (c) 49 kg/mol, respectively. (d) Separation height  $\Delta h$  as the function of wetting time for elastomers swollen with different molecular weight oils near their maximum;  $Q_{max} = 4.1$  (black, 14 kg/mol), 3.5 (blue, 28 kg/mol) and 2.3 (purple, 49 kg/mol).

In addition to the separation size, we can make a comparison of the time-dependent, oil separation dynamics from Fig. 5d for the different viscosities. For all samples, the oil separation occurs fastest in the early stages of wetting, which is then followed by a slower rate of oil separation. Qualitatively, one can observe that the early-stage oil separation occurs faster with lower viscosity oil. For example, the slope (separation height growth rate) of the curves in Fig. 5d in the first 1500 s (25 minutes) increase with decreasing molecular weight. This is intuitive if we consider that the oil mobility will scale inversely with the molecular weight. On the other hand, the growth slows down after a certain point in time, suggesting two regimes.

Description of separation process. Based on our experimental findings, it is clear that the separation process is associated with both the molecular weight of the swelling oil and the swelling ratio. The timescale of the separation process is relatively long, suggesting that it is dominated by diffusion. Given the time scales of our experiments, it is safe to consider that the system reaches the diffusion limit. To describe the phase separation growth dynamics, we consider that the ridge

grows through the accumulation of oil near the three-phase contact line, and that the oil is supplied by a diffusive flow through the swollen network. To describe the process, we set up a simple diffusion model for the growth of the wetting ridge in the presence of a drop. A key part of a theoretical description of the process is the driving force for the accumulation of oil in the ridge. The accumulation of oil is driven by differences in chemical potential between the ridge and the network outside the three-phase contact line. The ridge chemical potential can be obtained from the free energy in the ridge. We consider the ridge to be composed of the elastic network and the phase-separated oil, located at the three-phase contact line. The ridge free energy  $F_r$  depends on the number of chains  $n_r$  in the ridge and will be a complicated expression with contributions from the elasticity of the network, interfacial tensions, and possibly other contributions. Developing a comprehensive theory for the ridge free energy goes beyond the scope of the present work. Instead, we approximate the free energy function by an expansion about its minimum, which corresponds to the saturated ridge with  $n_0$  chains:

$$F_r \propto (n_r - n_0)^2$$
 (Eq. 1)

where  $n_r$  is the number of chains in the ridge and  $n_0$  is the number of chains at saturation, which is unknown. We consider the location of the ridge to be at the three-phase contact line radius R, and express the ridge free energy in terms of the line number density in the contact line

$$F_r = \int dl \frac{\kappa}{2} (\lambda - \lambda_0)^2 \quad \text{(Eq. 2)}$$

where  $\lambda \propto n_r/R$  and  $\lambda_0 \propto n_0/R$  are the actual line density and the line density at saturation respectively, R is the radius of the three-phase contact line, and  $\kappa$  is an unknown proportionality constant. The above-mentioned details of the physics in the ridge are captured implicitly within the two free parameters  $\kappa$  and  $\lambda_0$ . The details of the free energy in the ridge, however, should not play a major role, since the time evolution is dominated by slow diffusion.

For the free energy of the swollen polymer network, we include contributions from the translational entropy of the oil, in addition to a term relating to the elasticity of the network. The equilibrium free energy for the network is then chosen as

$$F_G = F_{id} + F_{el}$$
 (Eq. 3)

where  $F_{id}$  is the entropic contribution and  $F_{el} \propto Q^2$  is the elastic contribution. To capture the local details in the network, the free energy can be expressed in functional form, which depends on the local fraction of oil at different positions within the network. Expressed in this way, the free energy takes the form

$$\mathcal{F}_{G}[\varphi] = \iiint_{\Omega}^{\square} dV \left\{ \frac{\varphi}{N_{o}} \left( \ln \varphi - 1 \right) + \frac{K}{2} \frac{1}{1 - \varphi} \right\} (Eq. 4)$$

where the integral is evaluated over the volume of the network,  $N_o$  is the number of repeat units per oil chain,  $\varphi$  is the local fraction of oil, and K is the elasticity of the network. The first term in Eq. 4 is the entropic contribution of the oil, while the second term is the contribution from elasticity.

Equilibrium between the ridge and network is achieved when the chemical potentials in both are equal. The equilibrium line density  $\lambda_e \leq \lambda_0$  is then given by

$$\lambda_e \equiv \lambda_0 + \frac{\mu_G^{eq}}{\kappa}$$
. (Eq. 5)

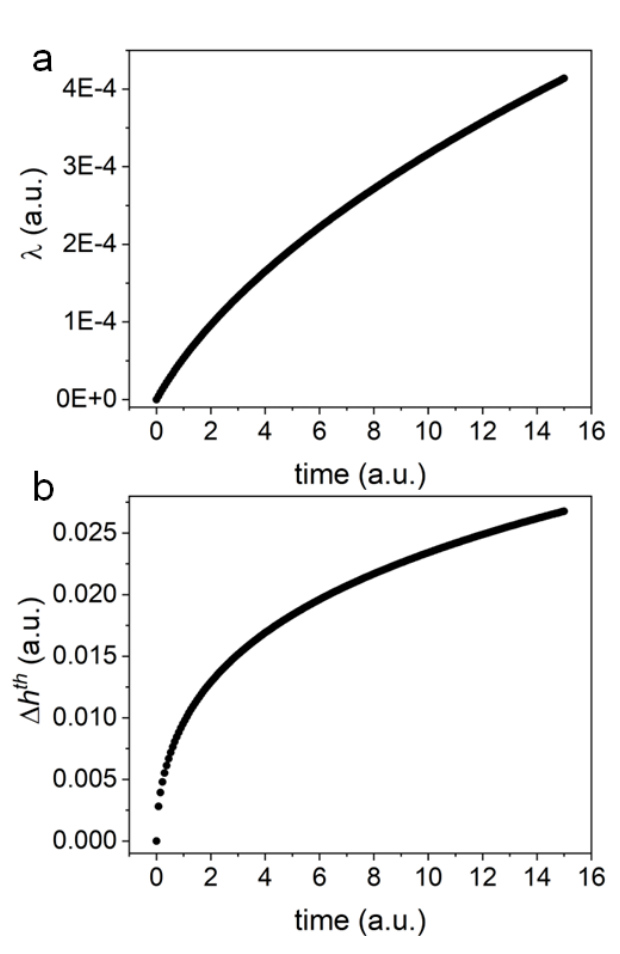


Figure 6. (a)  $\lambda(t)$  vs time as the direct result of solving the dynamical equations. (b) The separation height as calculated using  $\lambda(t)$  in Eqs. 9 and 10.

Here  $\mu_G^{eq}$  is the equilibrium chemical potential of the elastomer, which is negative and increases monotonously with  $\varphi$  and  $N_o$ . This means that when the swelling or the molecular weight of the

oil increases, more material will accumulate in the ridge at equilibrium. This provides theoretical support for the observations made earlier in Fig. 5.

For the out of equilibrium situation, having the expressions for the free energies of the ridge and the network enables us to derive dynamic equations. At the ridge, the flux  $j_r$  into the ridge is driven by the difference in chemical potential between the ridge and the network

$$j_r \propto \mu_r - \mu_G$$
. (Eq. 6)

Within the network, the local flux  $j_G$  is driven by local gradients in chemical potential. Using variational calculus, Eq. 4 can be varied to obtain the local flux  $j_G$  at every point within the network, in a fashion similar to Fick's first law. Combining the flux with a continuity equation results in a diffusion equation for the local fraction of oil within the network

$$\partial_t \varphi = M \nabla_r \left\{ \left[ \frac{1}{N_o} + \frac{K \varphi}{(1 - \varphi)^3} \right] \nabla_r \varphi \right\} . (Eq. 7)$$

Since our focus is on the separation rate, we assume that the liquid separates immediately from the network upon the formation of the ridge. With this assumption and since no material is lost during the growth of the ridge, any oil leaving the network must accumulate in the pure liquid ridge. With this we set up our diffusion equation with the appropriate boundary conditions, namely

$$j_G = -j_r$$
. (Eq. 8)

The full details on the derivation of the theoretical model are included in the Appendix. The diffusion equation with the boundary condition does not admit analytical solutions; we use a simple spatial discretization and integrate it with a forward Euler scheme.

Solving the dynamical equations gives us the line density within the ridge as a function of time  $\lambda(t)$ . An example of a solution is shown in Fig. 6a. To compare the results from the theory to the experiment, it is necessary to calculate the separation height from the line density. To accomplish this, we first calculate the volume of the phase-separated ridge from  $\lambda(t)$  as

$$V(t) = \frac{2\pi R\lambda(t)N_o}{\rho} \text{ (Eq. 9)}$$

where  $\rho$  is the density of the liquid and  $N_o$  is the number of repeat units per chain. As noted earlier in Fig. 4, the shape of the phase-separated ridge shows geometrically similar growth. This kind of growth can be exploited to calculate the separation height from the volume of the ridge without having a detailed shape for the ridge. The similarity assumption, combined with the fact

that the radius of the contact line (~mm) is much larger than the size of the ridge (~ $\mu$ m), implies that the volume scales quadratically with the height of the ridge  $V(t) \propto \Delta h^2(t)$ . As time progresses, the height of the ridge scales up by a factor of  $\alpha(t) = \Delta h(t)/\Delta h_0$ , where  $\Delta h_0$  is a reference height at a time  $t_0$ . We then have for the scaling factor  $\alpha(t) = \sqrt{V(t)/V_0}$ , where  $V_0$  is the volume at time  $t_0$ . This finally allows us to relate the separation height to the volume of the liquid ridge

$$\Delta h(t) = \Delta h_0 \sqrt{\frac{V(t)}{V_0}}. \text{ (Eq. 10)}$$

Using Eqs. 9 and 10 we can calculate the separation height  $\Delta h(t)$  from  $\lambda(t)$  as shown in Fig. 6b.

With the goal of comparing our experimental data to this simplified theory, we solve the diffusion equation for a given set of fixed parameters (e.g. modulus of the material and the drop size, details in the Appendix) and vary the molecular weights and swelling ratios; these are chosen based on the molecular weight and swelling ratios from experiments. The parameter that appears in the theory is the degree of polymerization of the oil  $N_o$ . For the 14, 28, and 49 kg/mol oils,  $N_o$  values are set to 184, 378, and 667 respectively, assuming a repeat unit (monomer) molar mass of 74 g/mol. The mobility in the theory is taken as  $M = M_0/N_o$ , such that it scales inversely with the molecular weight and  $M_0$  is the mobility of an individual monomer. This assumes that there is no effect of entanglements. In the diffusion regime, the only effect of entanglements is that the mobility M varies more strongly with molecular weight  $M_w$ . 58 When it comes to inter-chain entanglements, an estimation of the entanglement molecular weight  $M_c$  for PDMS yields  $M_c$  =  $33 \pm 7$  kg/mol.<sup>59</sup> A study of the transition between the two regimes shows that it can be smooth.<sup>60</sup> The 14 kg/mol is below  $M_c$  while the 28 kg/mol falls is within the confidence interval from below, and we will consider both to not have entanglements. The mobility of the 49 kg/mol oil might include effects from entanglements. However, given the smoothness of the transition and that the molecular weight is not too far above the  $M_c$  value confidence obtained by Valles and Macosko<sup>59</sup>, we assume that inter-chain entanglement plays a small role and will be neglected. Moreover, for elastomers prepared from commercial kits as we do here, it is difficult to estimate the density of crosslinks and strand lengths, which are relevant for determining the properties of the swollen elastomer.<sup>61</sup> Previous studies on the diffusion of unreactive PDMS chains in PDMS networks found that up to weight average molecular weights of 30 kg/mol, Rouse dynamics still govern the diffusion.<sup>62,63</sup> Taking this into consideration, we use the scaling  $M \propto \frac{1}{M_{W}}$  for our mobility.

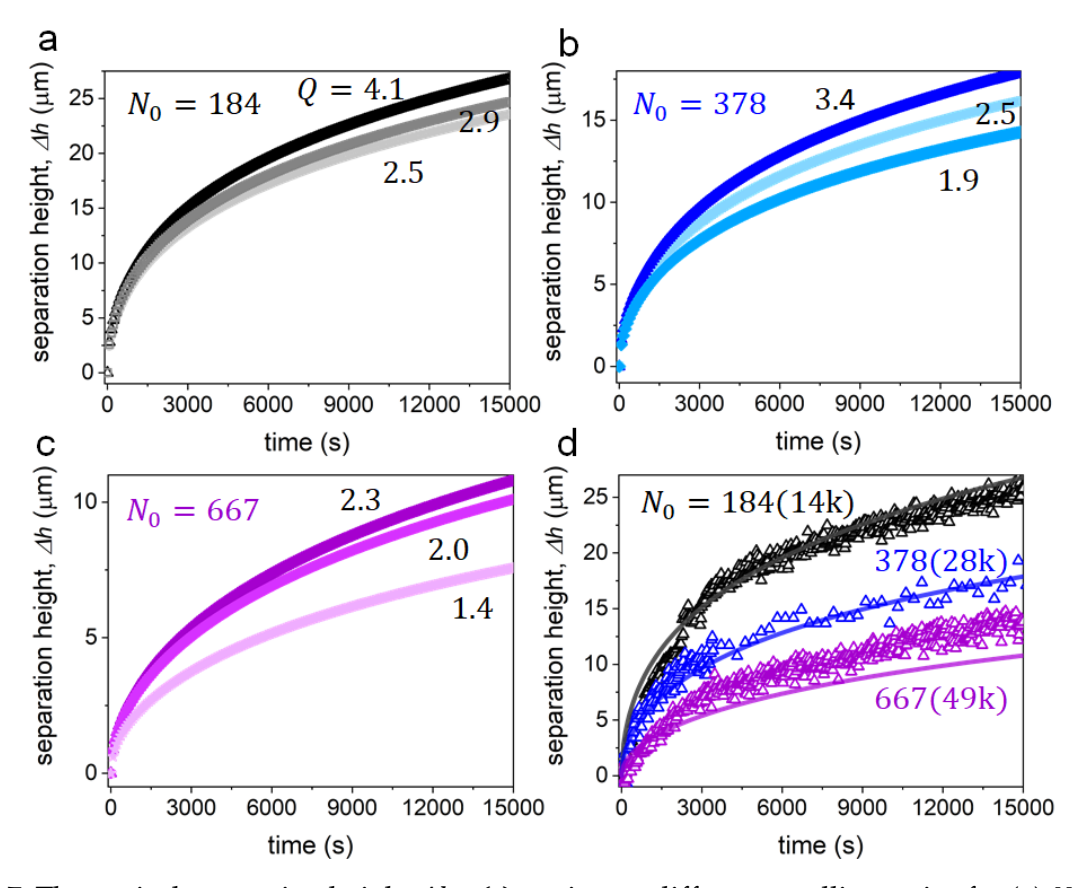


Figure 7: Theoretical separation height  $\Delta h_{th}(t)$  vs time at different swelling ratios for (a)  $N_o$  = 184, (b)  $N_o$  = 378, (c)  $N_o$  = 667. (d) Same as a-c but for the highest swollen elastomers with oils of different molecular weights. The theoretical results are shown in solid lines, while the experimental results in triangles.

The results for the theoretical separation heights  $\Delta h_{th}$  are shown in Fig. 7, which is designed to be analogous to Fig. 5. Figs. 7a-c show the evolution of the separation height for  $N_o=184,378,667$  respectively, at different swelling ratios. One difference is apparent between the theory (Figs. 7a-c) and the experiments (Figs. 5a-c) for lower swelling ratios. In the experiments, we have little and quickly saturating growth for low swelling ratios, while in the theory the growth is significant and slow for all swelling ratios. Since the ridge heights reached for low swelling are much smaller than for high swelling, it is possible that all of the necessary oil is supplied from the immediate surrounding of the ridge, and equilibrium is reached before the diffusive regime sets in. One possible explanation for the discrepancy is our choice of parameters in the free energy for the ridge Eq. 3. We choose the same value for the proportionality constant  $\kappa$  and for the saturation line density  $\lambda_0$  while both could depend on the swelling ratio. For  $Q_{max}$  in particular, the theoretical curves are in good qualitative agreement with the experiments. This is illustrated in Fig. 7d, showing the evolution of the separation height for different molecular weights at the highest swelling ratios for both theory (lines) and experiment (triangles). Above we made the choice for the scaling law of the mobility as  $M \propto 1/M_w$ , based on observations from

the literature. <sup>62,63</sup> The agreement of the theory with the experiment in Fig. 7d supports the validity of this scaling.

To better quantify the similarities and differences we plot the data in a logarithmic scale and extract power law exponents of the form  $\Delta h \propto t^{\beta}$ . Figs. 8a and 8b show the data on a logarithmic scale for the experimental results and the theoretical results respectively, for different molecular weights at high swelling. The grey dotted lines in the plots are power law fits for the data at  $t \geq 7500$ s. It is clear in both the experiment and theory that different regimes exist at early and late stages, as evident from the deviation of the fit from the curves. The experimental exponents with standard errors are  $\beta_{ex} = 0.296 \pm 0.005$  (14 kg/mol),  $0.338 \pm 0.029$  (28 kg/mol), and  $0.489 \pm 0.016$  (49 kg/mol), while the theoretical exponents are  $\beta_{th} = 0.335$  ( $N_0 = 184$ ), 0.356 ( $N_0 = 378$ ), and 0.412 ( $N_0 = 667$ ). The experimental and theoretical exponents are in reasonably good agreement, suggesting that the mechanisms governing the long-term growth of the ridge are most likely simple diffusion and geometry.

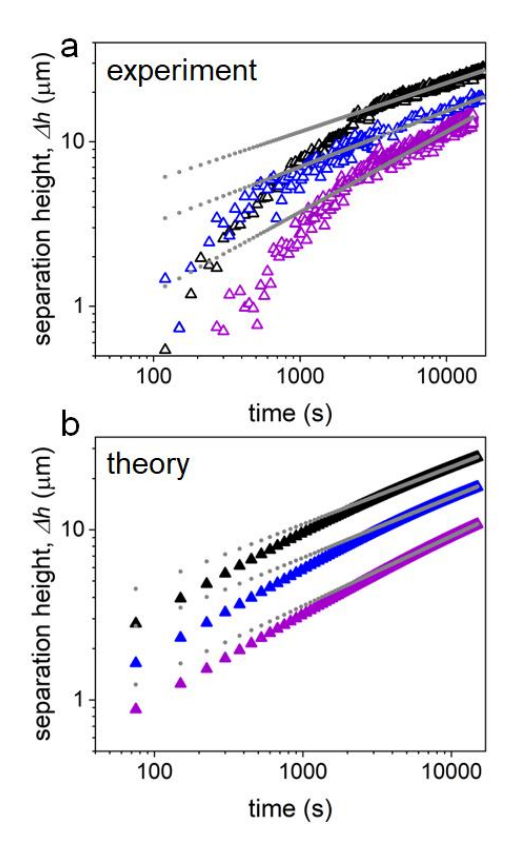


Figure 8. (a) Logarithmic plot of the experimental height vs. time for saturated elastomers with different oil molecular weights. The grey dots are power law fits with  $\Delta h \propto t^{\beta_{ex}}$  for  $t \geq 7500$  s.  $\beta_{ex} = 0.30$ , 0.34, and 0.49 for the 14 kg/mol, 28 kg/mol, 49 kg/mol molecular weight oils, respectively. (b) The same plots as part (a) but for the theoretical results. The grey dots are power law fits  $\Delta h \propto t^{\beta_{th}}$  for  $t \geq 7500$ s.  $\beta_{th} = 0.34$ , 0.36, and 0.41 for the monomer numbers of  $N_0 = 184$ , 378, and 667, respectively.

It is interesting to note that in the early-stage of phase separation growth, the rates are in the order 14k > 28k > 49k; this is observed in initial slopes of Fig. 5d, prior to reaching the second regime. On the other hand, the power law fits in Fig. 8 show the scaling exponents in the order of 49k > 28k > 14k. Evidently, the late-stage phase separation height grows faster with higher viscosity oils (e.g. 49k) compared to lower viscosity (e.g. 14k). This can be rationalized by considering the initial phase separation rate to be governed by two main two factors: (a) the swelling ratio is higher for lower molecular weight oils, meaning there is more oil available in the local vicinity and (b) a low viscosity permits faster oil flow. Hence, the 14k oil separates more and faster initially. For the late-stage separation, the slower rates for lower molecular weight oil would then be due to the phase-separated ridge being closer to equilibrium, such that the chemical potential difference is smaller.

#### Conclusions

In this study, we employ confocal microscopy to separately visualize the crosslinked network and the mobile oil of a swollen elastomer during wetting. When a drop is placed on the surface, we show that phase separation occurs near the contact line, where the phase separation dynamics is related to the molecular weight of the swelling oil and the degree of swelling. The ridge formation starts with a deformation of both components, followed by a quick separation of the liquid and subsequent relaxation of the polymer network. The liquid part of the phase separated ridge grows in a geometrically similar fashion The ridge outlines collapse at different times after rescaling. For low swelling ratios, the ridge reaches the plateau height relatively fast, while at the highest swelling ratios, complete equilibrium is not reached even after long times (i.e., ~15000-18000 s) Higher degrees of swelling and lower molecular weight oils lead to larger phase separation sizes and rates in the early-stage wetting while, the separation rate appears to be faster for high viscosity oil at later stages of wetting, likely because less oil has separated compared to the lower viscosity counterpart, leading to a lower chemical potential. We confirm this by employing a model based on diffusion and by considering the geometrically similar growth of the phase separated ridge. The results of the model fit the experiments well for the highest swelling ratio. The theory fails, however, to predict the low equilibrium heights and the ensuing fast equilibration at lower swelling ratios. This shortcoming is most likely due to simplicity of the theoretical considerations, where the two free parameters  $\kappa$  and  $\lambda_0$  are chosen to be independent of the swelling ratio or oil molecular weight. A detailed molecular theory may be needed to capture the complex physics in the ridge. The physics in the ridge and the details of what governs early-stage phase separation dynamics are still open questions for future consideration.

# **Experimental section**

The details of the preparation of thin, swollen PDMS films for confocal imaging is described in our previous work<sup>40</sup>. Briefly, Sylgard 184 (Dow) is used as our model polydimethylsiloxane (PDMS) elastomer with base/crosslinker of 60:1. Fluorescein O,O'-diacrylate (Sigma-Aldrich) with concentration of ~400  $\mu$ g per gram of PDMS is used to dye the crosslinked PDMS network. The samples are cured in a 65°C oven for 48 hours, followed by extracting uncrosslinked chains

with hexane. After extraction, silicone oil that is mixed with a red-shifted perylene monoimide (PMI) dye is used to reswell the PDMS. In this work, silicone oil (polydimethylsiloxane, trimethylsiloxy terminated, Gelest) with viscosities of 350, 1000, or 5000 cSt are used. During reswelling, a minor amount of hexane can be used to help increase the swelling rate of viscous silicone oil into PDMS network. The silicone oil is mixed with hexane with a volume ratio of 1:8, and the oil-hexane mixture is added directly onto the extracted PDMS film. The oil-hexane mixture spontaneously swells into the PDMS network, and the degree of swelling is controlled by the volume of oil-hexane mixture added. The container with samples is sealed with aluminum foil for 1 week, followed by unsealing the container and leaving the samples in the open environment for 1 hour to allow any residual hexane to evaporate.

Confocal images are captured on an inverted confocal microscope (Leica SP8) equipped with a 40x objective with a correction ring. Two lasers with wavelengths of 488 nm and 638 nm are utilized to excite the fluorescein and PMI dyes separately, and two high-sensitivity (HyD) detectors are used to collect emission wavelength ranges of 500-600 nm and 670-750 nm. A 2  $\mu$ L glycerol drop is placed on the sample and cross-sectional images of the surface deformation are taken every 30 s or 10 mins, depending on the wetting time of the experiment. The heights of oil and network are measured by the vertical distance between the flat surface and the highest tip of the oil and network through MATLAB and image analysis.

## Appendix: Theoretical model

# Ridge model

List of symbols:

- $F_r$ : total free energy in the ridge
- $f_r$ : line free energy density of the ridge
- $\partial \Omega$ : contact line between the droplet and the swollen elastomer
- $\kappa$ : prefactor controlling the "rigidtity" of the free energy (implicitly holds information over the combined effect of elasticity of the swollen elastomer, interfacial effects, osmotic pressure.)
- $\lambda$ : line number density in the ridge
- $\lambda_0$ : saturation line number density in the ridge.
- $n_r$ : number of polymer chains in the ridge
- $N_o$ : number of repeat units per chain
- $n_0$ : saturation number of polymer chains in the ridge

Since the ridge is located at the three-phase contact line we write the free energy  $\mathcal{F}_r$  as an integral over a line free energy density  $f_r$ 

$$\mathcal{F}_r(\lambda) = \oint_{\partial\Omega} f_r \, \mathrm{d}l \, (\text{Eq. A1})$$

where the integral is executed over the three-phase contact line of the droplet with the surface. We assume that the state of the ridge is not too far away from the equilibrium, so that it can be approximated by a quadratic function in the line number density in the ridge  $\lambda$ 

$$f_r(\lambda) = \frac{1}{2}\kappa(\lambda - \lambda_0)^2$$
 (Eq. A2)

with  $\lambda_0$  the line density at saturation. The total number of polymer chains in the ridge is

$$n_r = \frac{1}{N_o} \oint_{\partial \Omega} \lambda \, dl \, (\text{Eq. A3})$$

with  $N_o$  the number of repeat units per chain. With this, the total free energy of the ridge can also be written in terms of the number of chains, up to a numerical prefactor that depends on the radius of the droplet and  $N_o$ 

$$\mathcal{F}_r \propto (n_r - n_0)^2 \text{ (Eq. A4)}$$

with  $n_0$  the number of chains at saturation.

### Swollen elastomer model

List of symbols:

- $\varphi(r,z)$ : local lubricant fraction in swollen elastomer
- $h_0(r)$ : local height of the swollen network
- $\varphi_b$ : initial fraction of lubricant in network
- $H_0$ : height of collapsed network (no lubricant)

- *K*: elastic constant
- $\mathcal{F}[\varphi,\lambda]$ : total free energy functional
- $N_o$ : number of repeat units per chain
- $\Omega$ : the spacial domain of the swollen network

We consider a situation where the lubricant swells an elastomeric layer, and the elasticity of the swollen network layer contributes to the dynamic equation. We formulate the theory in terms of the bulk density  $\varphi(r,z)$  inside the swollen network, where z is the coordinate perpendicular to the surface layer, and r the radial coordinate. We will assume that the layer is thin enough that the perpendicular lubricant diffusion is very fast, hence  $\varphi(r,z) = \varphi(r)$  only depends on r. For given layer thickness H we have the relations:

$$\Phi(r) = \int_0^H \mathrm{d}z \; \varphi(r,z) = h_0(r) \; \varphi(r), \qquad h_0(r) = \frac{H_0}{\left(1 - \varphi(r)\right)}. \text{(Eq. A5)}$$

The total free energy of the system has an elastic contribution due to the swelling of the network. The elastic distortion is described in terms of a strain tensor  $\mathbf{\varepsilon}$ , which is derived from the displacement  $\vec{u}(\vec{r}_0) = \vec{r} - \vec{r}_0$  of a point in the swollen network with respect to its position  $\vec{r}_0$  in the unswollen reference network. Here we only account for swelling in the z direction, therefore the strain tensor only has one nonzero component  $\varepsilon_{zz} = \partial u_z/\partial r_{0,z} \approx \partial z/\partial z_0 = 1/(1-\varphi)$ . In coordinates  $z_0$  of the unswollen network, the elastic energy can then be written as  $\mathcal{F}_{el} = \frac{\kappa}{2} \int_0^H \mathrm{d}\,z\, \varepsilon_{zz}$ . In coordinates of the swollen network, this can be written as  $\mathcal{F}_{el} = \frac{\kappa}{2} \int_0^H \mathrm{d}\,z\, \varepsilon_{zz}$ . The

integral gives  $\mathcal{F}_{el} = \frac{K}{2}H^2/H_0 \propto H^2$  as expected. Hence, we obtain the total free energy

$$\mathcal{F}[\varphi,\lambda] = \iint_{\Omega} dA dz \left\{ \frac{\varphi}{N_{\varrho}} \left( \ln \varphi - 1 \right) + \frac{K}{2} \frac{1}{1 - \varphi} \right\} + \oint_{\partial \Omega} dl f(\lambda) \text{ (Eq. A6)}$$

where the first term in the first integral is the entropic contribution, and the second integral is the contribution of the ridge from the previous section.

### **Dynamic equations**

List of symbols:

- $\vec{j}_G$ : lateral diffusive current in the network
- $\vec{j}_r$ : diffusive current into the ridge
- *M*: Mobility of the lubricant chains
- *B*: fill rate at the ridge
- $\mu_G^{eff}$ : effective chemical potential in the network
- $\mu_G^{eq}$ : equilibrium chemical potential in the network

The lubricant density  $\varphi$  obeys the continuity equation  $\partial_t \varphi + \nabla \vec{j} = 0$ , but the current  $\vec{j}$  has a diffusive and a convective component. The convective component is perpendicular to the substrate and describes the lubricant transport with the swollen network as it expands. Given our

assumption that  $\varphi(r,z)$  does not depend on z due to the joint effect of convection and fast perpendicular diffusion, we do not need to calculate it explicitly. The diffusive current in the lateral direction is given by

$$\vec{J}_G = -M\varphi\nabla_r \frac{\delta\mathcal{F}}{\delta\varphi} = -M\left\{\frac{1}{N_o} + \frac{K\varphi}{(1-\varphi)^3}\right\}\nabla_r\varphi.$$
 (Eq. A7)

The flux into the ridge is driven by a difference in effective chemical potentials at the boundary  $\partial \Omega \equiv r = R$ . In addition, it will be proportional to the fraction of lubricant present at the boundary  $\Phi(R)$ . Since material accumulates in the ridge, we have the following equation

$$\partial_t \lambda = -B \Phi(R) \left[ f'(\lambda) - \mu_G^{eff} \right]$$
 (Eq. A8)

with B a filling rate at the ridge. We make the approximation that the effective chemical potential in the swollen network near the ridge stays close to the equilibrium value and set  $\mu_G^{eff} = \mu_G^{eq}$ . At equilibrium the free energy of the swollen network is

$$\mathcal{F}_G^{eq} = n_o(\ln\varphi - 1) + \frac{K}{2} \frac{n_o N_o}{\varphi(1 - \varphi)} \text{ (Eq. A9)}$$

and the chemical potential is

$$\mu_G^{eq} = \frac{\partial \mathcal{F}_G^{eq}}{\partial n_o} = \ln \varphi - \varphi + \frac{KN_o}{1 - \varphi}$$
 (Eq. A10)

Hence, we have the set of equations

$$\partial_t \varphi = M \nabla_r \left\{ \frac{1}{N_o} + \frac{K \varphi}{(1 - \varphi)^3} \right\} \nabla_r \varphi \text{ (Eq. A11)}$$

$$\partial_t \lambda = -B \varphi(R) \left[ \kappa (\lambda - \lambda_0) - \mu_G^{eq} \right]. \text{ (Eq. A12)}$$

We can define the equilibrium line density in the ridge  $\lambda_e \equiv \lambda_0 + \frac{\mu_G^{eq}}{\kappa}$  and rewrite eq. A.12 as

$$\partial_t \lambda = -B \Phi(R) \kappa(\lambda - \lambda_e)$$
. (Eq. A13)

For the boundary conditions, we choose at the contact line an equal flux boundary condition, while at the outer boundary we choose constant volume fraction

$$-H(\varphi(R)) j_G(R) \stackrel{!}{=} \partial_t \lambda \text{ (Eq. A14)}$$
  
$$\varphi(\infty) = \varphi_b. \text{ (Eq. A15)}$$

The initial conditions are chosen as

$$\varphi(r,t=0) = \varphi_b$$
 inside  $\Omega$  (Eq. A16)  
 $\lambda(t=0) = 0$ . (Eq. A17)

Using eqs. A.5, A.7, and A.12, the boundary condition eq. A.14 can be written as

$$\left[\frac{H_0 M}{1 - \varphi} \left\{ \frac{1}{N_o} + \frac{K\varphi}{(1 - \varphi)^3} \right\} \nabla_r \varphi \right]_{r=R} = -B \Phi(R) \kappa(\lambda - \lambda_e). \text{ (Eq. A18)}$$

### Numerical integration

In order to solve the equation numerically, we split the domain radially into bins with width  $\Delta r$ , and label the separate bins as  $r_i$  with  $r_0 = R$ . For any function g(r) we call  $g_i \equiv g(r_i)$ . We use the

discretization scheme:

$$\frac{\partial g_i}{\partial r} = \frac{1}{2\Delta r} (g_{i+1} - g_{i-1}) \text{ (Eq. A19)}$$

$$\frac{\partial^2 g_i}{\partial r^2} = \frac{1}{\Delta r^2} (g_{i+1} + g_{i-1} - 2g_i) \text{ (Eq. A20)}$$

and the forward steps in time are executed as a forward Euler scheme.

The inner boundary condition is imposed by rewriting eq. A.18 in the following way and solving for  $\varphi(R) \equiv \varphi_0$ 

$$(\varphi_1 - \varphi_0) \left[ \frac{(1 - \varphi_0)^3}{N_0} + K \varphi_0 \right] - \frac{B}{M} \kappa (\lambda - \lambda_e) \varphi_0 (1 - \varphi_0)^3 \Delta r = 0 \text{ (Eq. A21)}$$

where we used a forward derivative definition instead of central derivative for the concentration at the ridge.

# Height of the ridge by geometric scaling

List of symbols:

- h(r, t): shape function of the ridge at time t
- $\Delta h(t)$ : separation height at time t
- $\alpha(t)$ : scaling factor  $\alpha(t) = \frac{\Delta h(t)}{\Delta h_0}$
- R: radius of the drop and position of the ridge tip
- V(t): volume of the ridge at time t

Due to the symmetry of the system, the total ridge is a solid of revolution traced by rotating a curve h(r - R, t) around the z-axis. The volume of the ridge is then

$$V(t) = 2\pi \int_0^\infty h(r - R, t) r dr. \text{ (Eq. A22)}$$

The position of the ridge  $R \sim \text{mm}$ , while the size of the ridge is on the order of  $10\mu\text{m}$ . That means that the shape function must decay very quickly as one moves away from r = R. Due to this, most of the contribution to the volume is coming from the region close to the tip, and the volume of the ridge is very well approximated by

$$V(t) = 2\pi R \int_0^\infty h(r - R, t) dr. \text{ (Eq. A23)}$$

Executing a change of variables r' = r - R the expression for the volume becomes

$$V(t) = 2\pi R \int_{-\infty}^{\infty} h(r', t) dr' \text{ (Eq. A24)}$$

where we extend the lower bound to  $-\infty$  since the radius R is much larger than the size of the ridge. From the confocal microscopy images, and the analysis in Fig. 4, the shape of the ridge

shows geometrically similar growth. We therefore choose a scaling form for the shape function h(r',t)

$$h(r',t) = \alpha(t)h\left(\frac{r'}{\alpha(t)}\right)$$
 (Eq. A25)

where  $\alpha(t)$  is a time-dependent scaling factor. Following another change of variable  $r' \to \alpha(t)r'$ in eq. A.24 the expression for the volume becomes

$$V(t) = \alpha^{2}(t)2\pi R \int_{-\infty}^{\infty} h(r')dr'$$

$$= \alpha^{2}(t)V_{0}$$
(Eq. A26)

where  $V_0$  is a constant with units of volume. We then see that the volume scales quadratically with the scaling factor. The scaling factor at time *t* is related to the height of the phase separated ridge  $\Delta h(t)$  through

$$\alpha(t) = \frac{\Delta h(t)}{\Delta h_0} \text{ (Eq. A27)}$$

where  $\Delta h_0$  is the height of the ridge when the volume is equal to  $V_0$ . Putting all this together we finally get

$$\Delta h(t) = \Delta h_0 \sqrt{\frac{V(t)}{V_0}}. \text{ (Eq. A28)}$$

The total volume can be obtained from the solution of the diffusion equation as

$$V(t) = \frac{N(t)}{\rho} = \frac{2\pi R\lambda(t)}{\rho}$$
 (Eq. A29)

where  $\rho$  is the density of the fluid. Having the volume V(t) and choosing for  $V_0$  and  $\Delta h_0$ , we use eq. A.28 to obtain the time evolution of the height.

### Parameters and units

The diffusion equation was solved for the following fixed parameters:

- R = 1
- $K = 0.4 \times 10^{-4}$
- $\kappa = 2.5$
- $\lambda_0 = 1$   $B = 12 \times 10^{-5}$

The mobility was chosen depending on the molecular weight of the fluid as  $M = \frac{M_0}{N_0}$  with  $M_0 =$  $10^{-3}$ . We chose  $N_o = 184,378,667$  which correspond to to the molecular weights of the oils in the experiment using 74 g/mol as the molecular weight of a monomer. For each  $N_o$  we chose three values for  $\varphi_b$  that would correspond to the experimental swelling ratios using  $\varphi_b = 1 - 1/Q$ . We choose discretized time and spacial steps  $\Delta t = 10^{-6}$ ;  $\Delta r = 2 \times 10^{-4}$ . For the values of  $V_0$  and  $\Delta h_0$  we choose the shape of the ridge to be an isoceles triangle with side length  $\approx 2R \times 10^{-4}$ . We choose  $\rho = 1$  in eq. A.29. A possible mapping of units is to identify the radius of the drop to R = 1 mm and the mobility  $M_0 = 10^{-12} \text{m}^2/\text{s}/k_B T$ , which sets the unit of time in the theory to  $[t] = 10^3$ s.

## Acknowledgements

The authors appreciate discussion with Doris Vollmer. This research is funded by the US National Science Foundation through CBET 2326933 and 2043732. Part of this research was funded by the German Science Foundation (DFG) within the priority program SPP 2171 (Grant No. 422796905, projects Schm 985/22) and the DFG Emmy Noether Programme No. 460056461. Further support is acknowledged from the DFG-funded Graduate School RTG 2516 (Grant No. 405552959): RGMB is an associated member, FS is a member.

### References

- 1 D. Rus and M. T. Tolley, *Nature*, 2015, **521**, 467–475.
- I. Sotiri, A. Tajik, Y. Lai, C. T. Zhang, Y. Kovalenko, C. R. Nemr, H. Ledoux, J. Alvarenga, E. Johnson, H. S. Patanwala, J. V. I. Timonen, Y. Hu, J. Aizenberg and C. Howell, *Biointerphases*, 2018, **13**, 06D401.
- 3 C. Urata, G. J. Dunderdale, M. W. England and A. Hozumi, *J. Mater. Chem. A*, 2015, **3**, 12626–12630.
- 4 N. Lavielle, D. Asker and B. D. Hatton, *Soft Matter*, 2021, 17, 936–946.
- 5 L. Chen, E. Bonaccurso, T. Gambaryan-Roisman, V. Starov, N. Koursari and Y. Zhao, *Curr. Opin. Colloid Interface Sci.*, 2018, **36**, 46–57.
- 6 B. Andreotti and J. H. Snoeijer, *Annu. Rev. Fluid Mech.*, 2020, **52**, 285–308.
- M. Zhao, F. Lequeux, T. Narita, M. Roché, L. Limat and J. Dervaux, *Soft Matter*, 2018, **14**, 61.
- 8 K. Chaudhuri and J. T. Pham, *Soft Matter*, 2022, **18**, 3698–3704.
- 9 A. Pandey, B. Andreotti, S. Karpitschka, G. J. van Zwieten, E. H. van Brummelen and J. H. Snoeijer, *Phys. Rev. X*, 2020, **10**, 031067.
- 10 M. Van Gorcum, S. Karpitschka, B. Andreotti and J. H. Snoeijer, *Soft Matter*, 2020, **16**, 1306–1322.
- J. Gerber, T. Lendenmann, H. Eghlidi, T. M. Schutzius and D. Poulikakos, *Nat. Commun.*, 2019, **10**, 4776.
- 12 M. Zhao, J. Dervaux, T. Narita, F. Lequeux, L. Limat and M. Roché, *Proc. Natl. Acad. Sci.*, 2018, **115**, 1748–1753.
- 13 H. K. Khattak, S. Karpitschka, J. H. Snoeijer and K. Dalnoki-Veress, *Nat. Commun.*, 2022, **13**, 4436.
- 14 A. Carré, J.-C. Gastel and M. E. R. Shanahan, *Nature*, 1996, **379**, 432–434.
- 15 L. Hauer, Z. Cai, A. Skabeev, D. Vollmer and J. T. Pham, *Phys. Rev. Lett.*, 2023, **130**, 058205.
- 16 Z. Cai and J. T. Pham, ACS Appl. Polym. Mater., 2022, 4, 3013–3022.
- 17 M. H. Essink, S. Karpitschka, H. K. Khattak, K. Dalnoki-Veress, H. van Brummelen and J. H. Snoeijer, *arXiv*, 2024, arXiv:2402.06344.
- 18 M. Oléron, L. Limat, J. Dervaux and M. Roché, *Soft Matter*, 2024, **20**, 762–772.
- 19 H. H. Tran, D. Lee and D. Riassetto, *Reports Prog. Phys.*, 2023, **86**, 066601.
- 20 J. Sun and P. B. Weisensee, *Soft Matter*, 2019, **15**, 4808–4817.
- 21 C. Semprebon, G. McHale and H. Kusumaatmaja, Soft Matter, 2017, 13, 101–110.
- F. Schellenberger, J. Xie, N. Encinas, A. Hardy, M. Klapper, P. Papadopoulos, H.-J. Butt and D. Vollmer, *Soft Matter*, 2015, **11**, 7617–7626.
- 23 R. G. M. Badr, L. Hauer, D. Vollmer and F. Schmid, J. Phys. Chem. B, 2022, 126, 7047–7058.
- 24 Q. Liu and Z. Suo, *Extrem. Mech. Lett.*, 2016, 7, 27–33.
- K. E. Jensen, R. Sarfati, R. W. Style, R. Boltyanskiy, A. Chakrabarti, M. K. Chaudhury and E. R. Dufresne, *Proc. Natl. Acad. Sci. U. S. A.*, 2015, **112**, 14490–14494.
- 26 W. S. Y. Wong, L. Hauer, A. Naga, A. Kaltbeitzel, P. Baumli, R. Berger, M. D'Acunzi, D.

- Vollmer and H.-J. Butt, Langmuir, 2020, 10.1021/acs.langmuir.0c00538.
- 27 H. Jeon, Y. Chao and S. Karpitschka, *Phys. Rev. E*, 2023, **108**, 024611.
- 28 M. Roché, L. Talini and E. Verneuil, *Langmuir*, 2024, **40**, 2830–2848.
- 29 S. Kaneko, C. Urata, T. Sato, R. Hönes and A. Hozumi, *Langmuir*, 2019, **35**, 6822–6829.
- 30 S. Nakamura, H. Kakiuchida, M. Okada and A. Hozumi, *Adv. Funct. Mater.*, 2024, 34, 2310265.
- 31 L. Hauer, A. Naga, R. G. M. Badr, J. T. Pham, W. S. Y. Wong and D. Vollmer, *Soft Matter*, 2024, **20**, 5273–5295.
- J. T. Pham, F. Schellenberger, M. Kappl and H.-J. Butt, Phys. Rev. Mater., 2017, 1, 015602.
- 33 Y. Hu, X. Zhao, J. J. Vlassak and Z. Suo, Appl. Phys. Lett., 2010, 96, 121904.
- 34 A. R. Kim, S. K. Mitra and B. Zhao, J. Colloid Interface Sci., 2022, 628, 788–797.
- 35 Q. Xu, L. A. Wilen, K. E. Jensen, R. W. Style and E. R. Dufresne, *Phys. Rev. Lett.*, 2020, **125**, 238002.
- 36 M. M. Flapper, A. Pandey, M. H. Essink, E. H. van Brummelen, S. Karpitschka and J. H. Snoeijer, *Phys. Rev. Lett.*, 2023, **130**, 228201.
- 37 Z. Shao and Q. Liu, Extrem. Mech. Lett., 2023, 101996.
- 38 Y. Lai and Y. Hu, Mech. Mater., 2021, 159, 103877.
- 39 J. Zhu and Q. Liu, J. Mech. Phys. Solids, 2023, 170, 105124.
- 40 Z. Cai, A. Skabeev, S. Morozova and J. T. Pham, Commun. Mater., 2021, 2, 21.
- 41 W. Qian, W. Zhao, T. Qian and Q. Xu, arXiv, 2023, arXiv:2312.09493.
- R. W. Style, C. Hyland, R. Boltyanskiy, J. S. Wettlaufer and E. R. Dufresne, *Nat. Commun.*, 2013, 4, 2728.
- 43 S. J. Park, B. M. Weon, J. S. Lee, J. Lee, J. Kim and J. H. Je, *Nat. Commun.*, 2014, **5**, 4369.
- 44 S. Karpitschka, A. Pandey, L. A. Lubbers, J. H. Weijs, L. Botto, S. Das, B. Andreotti and J. H. Snoeijer, *Proc. Natl. Acad. Sci.*, 2016, **113**, 7403–7407.
- 45 R. Roy, R. L. Seiler, J. A. Weibel and S. V. Garimella, *Adv. Mater. Interfaces*, 2020, **2000731**, 1–9.
- 46 D. R. Darby, Z. Cai, C. R. Mason and J. T. Pham, J. Appl. Polym. Sci., 2022, 139, e52412.
- 47 J. D. Glover, X. Yang, R. Long and J. T. Pham, Nat. Commun., 2023, 14, 2362.
- 48 J. D. Glover, C. E. Mclaughlin, M. K. Mcfarland and J. T. Pham, *J. Polym. Sci.*, 2020, **1**, 343–351.
- 49 A. Hourlier-Fargette, J. Dervaux, A. Antkowiak and S. Neukirch, *Langmuir*, 2018, **34**, 12244–12250.
- 50 A. D. Gruber, C. W. Widenhouse, S. Mathes and R. P. Gruber, *J. Biomed. Mater. Res.*, 2000, **53**, 445–448.
- 51 J. N. Lee, C. Park and G. M. Whitesides, *Anal. Chem.*, 2003, **75**, 6544–6554.
- C. S. Sharma, A. Milionis, A. Naga, C. W. E. Lam, G. Rodriguez, M. F. Del Ponte, V. Negri, H. Raoul, M. D'Acunzi, H. J. Butt, D. Vollmer and D. Poulikakos, *Adv. Funct. Mater.*, 2022, 32, 2109633.
- A. Hourlier-Fargette, A. Antkowiak, A. Chateauminois and S. Neukirch, *Soft Matter*, 2017, **13**, 3484–3491.

- J. D. Berman, M. Randeria, R. W. Style, Q. Xu, J. R. Nichols, A. J. Duncan, M. Loewenberg, E. R. Dufresne and K. E. Jensen, *Soft Matter*, 2019, **15**, 1327–1334.
- G. Bartalena, R. Grieder, R. I. Sharma, T. Zambelli, R. Muff and J. G. Snedeker, *Biomed. Microdevices*, 2011, **13**, 291–301.
- 56 S. A. Rahat, K. Chaudhuri and J. T. Pham, *Soft Matter*, 2023, **19**, 6247–6254.
- G. I. Barenblatt, *Scaling, Self-similarity, and Intermediate Asymptotics,* Cambridge University Press, 1996.
- L. Garrido, J. L. Ackerman and J. E. Mark, in *New Trends in Physics and Physical Chemistry of Polymers*, 1989.
- 59 E. M. Valles and C. W. Macosko, *Macromolecules*, 1979, **12**, 521–526.
- T. Kataoka and S. Ueda, Jountla Polym. Sci. Part C Polym. Lett., 1966, 4, 317–322.
- 61 Y. Li, M. Kröger and W. K. Liu, *Polymer (Guildf).*, 2011, **52**, 5867–5878.
- 62 A. N. Gent and R. H. Tobias, J. Polym. Sci. Polym. Phys. Ed., 1982, 20, 2317–2327.
- J. Marzan, B. Leclerc, N. Galandrin and G. Couarraze, Eur. Polym. J., 1995, 31, 803–807.